In Situ STM Studies of Electrochemical Growth of Nanostructured Ni Films and Their Anomalous IR Properties

Han-Chun Wang, Shi-Gang Sun,* Jia-Wei Yan, Hong-Zhou Yang, and Zhi-You Zhou

State Key Lab of Physical Chemistry of Solid Surfaces, Department of Chemistry, Xiamen University, Xiamen 361005, China

Received: August 16, 2004; In Final Form: November 28, 2004

We have extended the study of anomalous IR properties, which were initially discovered on nanostructured films of platinum group metals and alloys, to nanostructured films of nickel, a member of the iron group triad, and broadened the fundamental knowledge on this subject. Nanostructured thin films of nickel supported on glassy carbon [nm-Ni/GC(*n*)] were prepared by electrochemical deposition under cyclic voltammetric conditions, and the thickness of films was altered systematically by varying the number (*n*) of potential cycling within a defined potential range for electrodeposition. Electrochemical *in situ* scanning tunneling microscopy (STM) was employed to monitor the electrochemical growth of nanostructured Ni films. These *in situ* STM images illustrated that, along the increase of the film thickness, Ni films have undergone a transformation from layer structure to island structure and finally to lumpish arris structure. Investigations by *in situ* FTIR spectroscopy employing adsorbed CO as the probe revealed that these nanostructures of Ni films yield abnormal IR features, Fano-like IR features, and normal IR features, respectively. The IR bands of CO adsorbed on Ni thin films of a layer structure were inverted in their direction and enhanced in their intensity up to 15.5 times on an nm-Ni/GC(*4*) electrode. The Fano-like IR features, which are defined as a bipolar band with its negative-going peak on the low wavenumber side and its positive-going peak on the high wavenumber side, are observed for the first time on Ni thin films of an island nanostructure, i.e., at the nm-Ni/GC(*16*) electrode. IR features changed to normal absorption in CO adsorbed on the nm-Ni/GC(*25*) electrode, i.e., that with lumpish arris nanostructured Ni film of a larger thickness.

Introduction

Nanomaterials are attracting ever increasing attentions among multidisciplinary researches in recent years because of their novel properties and potential applications in electronics,[1] optics,[2] catalysis,[3] ceramics,[4] and magnetic data storage.[5] In comparison with corresponding bulk materials, nanomaterials exhibit interesting and peculiar properties, for example, size- and shape-dependent catalytic activities,[6] novel mechanical behavior,[7] unique magnetic phenomena,[8] crystal-shape-dependent thermodynamics,[9] and quantum confinement phenomena.[10] It is well-known that such unique properties and improved performances are by and large determined by their size, structure, and mutual interaction between nanoparticles.[11]

In nanomaterials, anomalous optical properties are ubiquitous phenomena. For example, for almost all metals, the surface covered by nanoparticles would lose their luster and turn to black, as well as show a blue-shifted[12] absorbance. These phenomena are a part of nanomaterial optical properties generated primarily from peculiar quantum confinement and surface effects. Tabagi et al.[13] found that Si nanoparticles with a size of less than 6 nm could emit visible light when excited by ultraviolet light and considered it to arise from quantum confinement effects. Undoubtedly, further studies of optical properties of nanomaterials would yield exciting phenomena and contribute to future developments.

The progress of vibration spectroscopy in recent years also closely relates to the nanomaterial evolvement. The generation and enhancement of surface enhanced Raman scattering (SERS)[14] and surface enhanced IR absorption (SEIRA)[15] are both considered to arise from the size and separation of surface nanoscale islands. Likewise, surface-enhanced second harmonic generation (SESHG)[16] and surface-enhanced sum frequency generation (SESFG)[17] are both strongly dependent on the structure of nanomaterials.

Recently, Sun and co-workers[18−27] have revealed that nanostructured films exhibit anomalous IR absorbance characteristics of CO [and other spices, such as SCN-, poly-*o*-phenylenediamine (POPD), etc.], adsorbed on electrodes of nanostructured thin films of platinum group metals (Pt, Pd, Ru, and Rh) and their alloys (PtPd and PtRu); the major IR band of these adsorbates on nanostructured surfaces exhibits unusual changes in comparison to that of the same species adsorbed on corresponding bulk metal electrodes. The unusual changes of the IR band involve the inversion of the absorbance direction, significant intensity enhancement, and width broadening of the IR bands of the corresponding adsorbates on a nanostructured surface. These anomalous IR properties are observed both at solid/liquid and solid/gas[27] interfaces. Altogether these anomalous IR properties are referred as the abnormal IR effects (AIREs) of nanostructured films.[23,27] Similar AIREs of nanostructured films of Ir,[28] Os,[29] and platinized platinum[30] are also confirmed by other research groups. These discoveries of AIREs have attracted much attention and curiosity from relevant fields.[31,32] Our group[33] has investigated Pt thin films prepared by fast potential cycling treatment with varying durations and observed that, with the increase of Pt film thickness and island sizes, the direction and shape of the CO_L band is shifted from

* To whom correspondence should be addressed. Telephone: 86-592-2180181. Fax: 86-592-2183047. E-mail: sgsun@xmu.edu.cn.

10.1021/jp046313o CCC: $30.25
Published on Web 02/15/2005

the downward (normal IR features) and monopolar to bipolar mode (Fano-like IR features) and finally inverted to the upward and monopolar mode (anomalous IR effects). Similar results were obtained for Ru thin films prepared by electrodeposition on glazed Pt.[34]

As an important member of the iron group triad, Ni and its compounds are widely used in hydrogen storage,[35] catalysis,[36] battery components,[37] and certain functional materials.[38] It is well-known that, when CO is adsorbed on the Ni surface, a linearly bonded CO (CO_L, ~2090−1960 cm^{-1}) and a bridge-bonded CO (CO_B, 1960−1850 cm^{-1}) species are normally produced.[39] The present work is undertaken to extend the study of anomalous IR behavior, which has been discovered initially with platinum group metals and alloys, to iron group metals. Thus, we envisage broadening further the relationship between anomalous IR features and structures of films. Ni nanometer thin films were prepared by electrochemical deposition, and their structures were monitored and characterized with an electrochemical *in situ* scanning tunneling microscopy (STM). Herein, using CO adsorption as the probe indicator and monitored with *in situ* Fourier transform infrared reflection (FTIR) spectroscopy, the anomalous IR properties of nanostructured Ni thin films are reported.

Experimental Procedures

Preparation of Nanostructured Nickel Thin Films. Nickel thin films were prepared by electrochemical deposition, under potential cycling conditions, on a glassy carbon (GC) substrate of 6 mm in diameter (with a geometric area of 0.28 cm^2). The GC was sealed into a Teflon holder and polished mechanically by using successively sand paper (6#) and alumina powder of sizes 5, 1, 0.3, and 0.05 μm. The electroplating solution contains 0.1 mol L^{-1} Na_2SO_4 and 0.02 mol L^{-1} $NiSO_4$. The lower and upper potential limits for potential cycling were respectively −1.15 and −0.7 V (versus SCE), and the potential scan rate was 50 mV s^{-1}. A series of Ni films with different structure and thickness was prepared by varying the number (n) of potential cycles and is denoted as nm-Ni/GC(n). An EG&G potentiostat/galvanostat (model 263A) was employed in electrochemical studies. A saturated calomel electrode (SCE) served as a reference electrode, and a platinized platinum foil was used as a counter electrode. Millipore water (18 MΩ cm) obtained from a Milli-Q lab equipment (Nihon Millipore Ltd.) was used in preparation of the solution and the rinse of glassware and electrodes. All solutions were deaerated by bubbling high-purity N_2 before measurements.

Electrochemical *In Situ* STM. Electrochemical *in situ* STM studies were carried out using a Nanoscope IIIa (Digital Instruments) operated under the constant current mode. The investigation was carried out in a three-electrode system, in which nm-Ni/GC(n) was used as the working electrode, Pt wire as the counter electrode, and a freshly made Ag/AgCl as the reference electrode. To facilitate the discussion, electrode potentials reported thereafter were normalized to the SCE scale. Electrochemically etched and polyethylene-coated W tips were used in the study. The nm-Ni/GC(n) electrodes prepared in an *in situ* STM cell were performed under the same conditions as those made in a conventional cell in cyclic voltammetry (CV) and *in situ* FTIR investigations. *In situ* STM images were acquired in 0.02 mol L^{-1} $NiSO_4$ and 0.1 mol L^{-1} Na_2SO_4 solutions at −0.75 V. It has been confirmed that, through experimental fact, STM images of a given nm-Ni/GC(n) scanned consecutively at −0.75 V were identical and the nm-Ni/GC(n) electrode is stable at −0.75 V.

Electrochemical *In Situ* FTIR Spectroscopy. Electrochemical *in situ* FTIR spectroscopic studies were performed on a Nexus 870 spectrometer (Nicolet) equipped with a liquid-nitrogen cooled MCT-A detector and an EverGlo IR source. A CaF_2 disk was used as the IR cell window, and an nm-Ni/GC-(n) electrode was pushed against the IR window to create a thin layer of a few micrometers thickness for *in situ* FTIR measurements. The infrared radiation from the IR source passed through the CaF_2 window and the thin-layer solution and then reflected from the surface of the nm-Ni/GC(n) electrode. The infrared spectra were collected using either MSFTIRS[40] or SNIFTIRS[41] procedures. The resulting spectra are reported as the relative change in reflectivity, i.e.

$$\frac{\Delta R}{R} = \frac{R(E_S) - R(E_R)}{R(E_R)} \quad (1)$$

where $R(E_S)$ and $R(E_R)$ are single-beam spectra of the reflection collected at sample potential E_S and reference potential E_R, respectively. The spectral resolution was 8 cm^{-1}.

Results and Discussion

1. *In Situ* STM Studies. STM images of nm-Ni/GC(n) were scanned at −0.75 V immediately after the electrodeposition of Ni films with an appropriate number of potential cycles (n = 1, 4, 12, 16, and 25). As shown by *in situ* STM images in Figure 1, the structure of Ni thin films obviously depends on n. These Ni thin films can be regarded as a kind of two-dimensional nanomaterial that is composed of nanometer-sized particles. The film thickness ranges from a few nanometers to few hundred nanometers. Figure 2 displays three-dimensional structures of three distinctively different nm-Ni/GC(n) surfaces as illustrated by the *in situ* STM images, namely, for $n < 16$, $n = 16$, and $n = 25$. For the first case shown in the top row of Figure 1 where n = 1, 4, and 12, layer-shaped crystallites are formed on the thin film showing an average size of 30−120 nm in width and 2−10 nm in height; their length may extend to 700 nm. For the second case of $n = 16$, the film surface contains crystallites with island structures measuring 100−200 nm in width, 250−400 nm in length, and 15−30 nm in height. Finally, when n = 25, the film surface is dominated with relatively disordered, rugged lumpish arris crystallites, which are similar to the structure of the rough surface of a bulk Ni electrode.

As shown in Figure 3 and Table 1, Ni films grow thicker as n increases. The relationship between the estimated thickness (d_e) of Ni films and n is plotted in Figure 3 in which d_e is estimated by the following equation: [27]

$$d_e = \frac{Q_d N_0 V_{Ni}}{2FA_{GC}74.05\%} \quad (2)$$

where Q_d is the electric charge consumed in electrodeposition of Ni onto GC ($Ni^{2+} + 2e^- \rightarrow Ni$) and has been measured from the integration of $j-E$ curves recorded in electrodeposition. Also, F is the Faraday constant, N_0 is Avogadro's number, V_{Ni} is the volume of one Ni atom ($V_{Ni} = {}^4/_3\pi r_{Ni}^3$), and A_{GC} is the geometric area of GC substrates. The operation of eq 2 is based on the assumption that the efficiency of electrodeposition of Ni is 100% and that Ni atoms are arranged as the close cubic packing to yield space occupancy of 74.05%. The d_e increases linearly with the increase of n (Figure 3). It should be pointed out that the real thickness of electrodeposited Ni film might be much larger than d_e, because the Ni atoms electrodeposited onto GC substrates could not be perfectly cubic close packed.[27] As

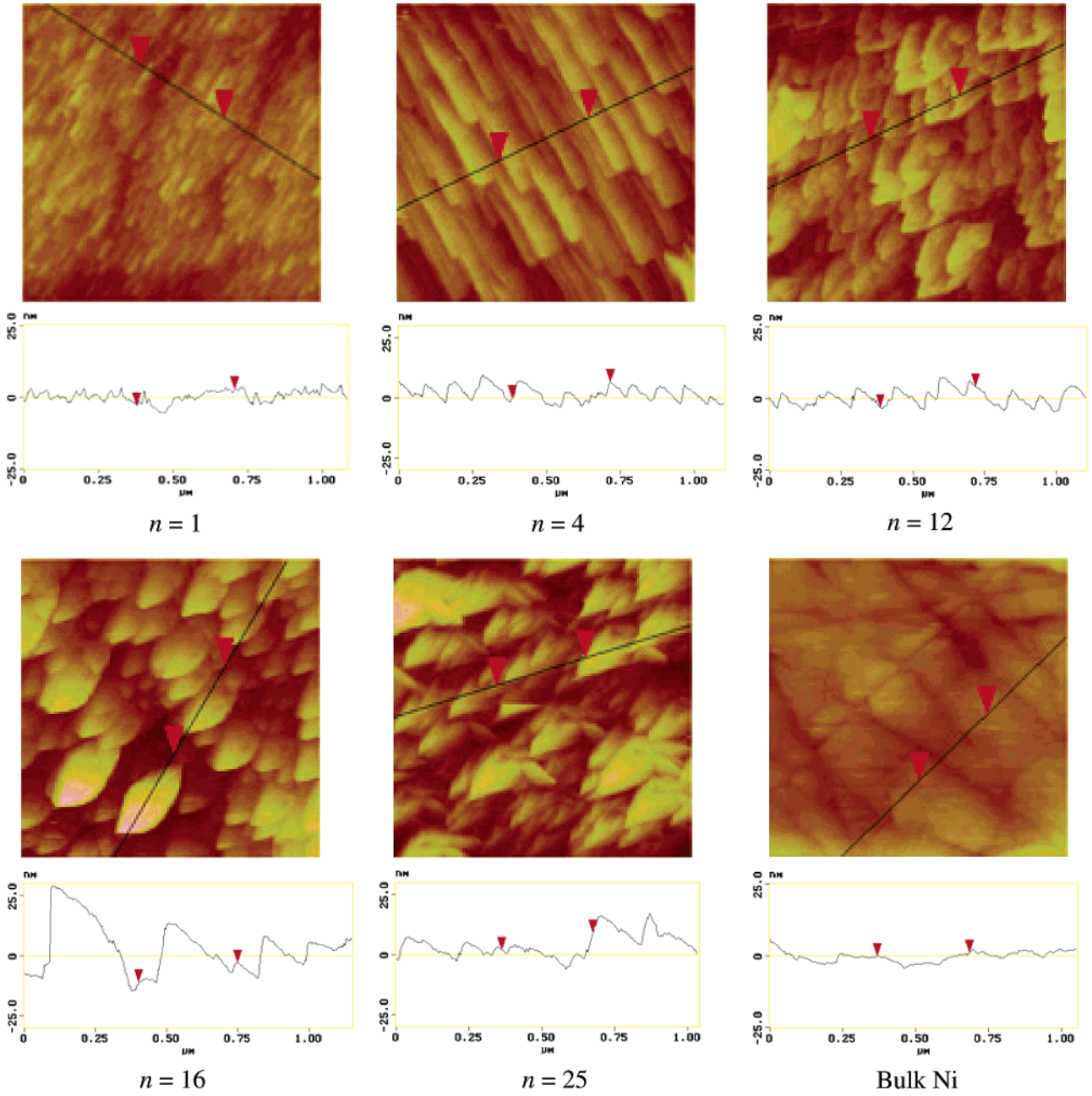

Figure 1. *In situ* STM images of nm-Ni/GC(*n*) with $n = 1$, 4, 12, 16, and 25 and bulk Ni at −0.75 V, respectively. Scan size = 1 × 1 μm. *Z* range = 60 nm. Solution = 0.1 mol L^{-1} Na_2SO_4 and 0.02 mol L^{-1} $NiSO_4$.

shown by STM images, all surfaces of nm-Ni/GC(*n*) are rougher than a rough surface of bulk Ni that makes the real thickness of the former surfaces larger than the estimated d_e, although still within the nanometer range. Thus, in the present study, both *n* and d_e can be used as a relative parameter, that is, in direct proportion to the thickness of nanostructured Ni films.

Table 2 lists the mean square root roughness (R_q) of Ni films and bulk Ni measured by *in situ* STM. R_q represents the standard deviation of the *z* value in the measured area that for nm-Ni/GC(*1*) is only 2.4 nm, which is close to the value of bulk Ni mechanically polished by using 50 nm Al_2O_3 polishing powders. R_q slightly increases from 2.4 to 4.2 nm with *n* increasing from 1 to 12 and sharply increases when $n > 12$.

2. Cyclic Voltammetric Studies. A newly electrodeposited nm-Ni/GC(*n*) electrode was first subjected to a potential cycling between −1.0 and −0.8 V with bubbling high-purity N_2 into solution for at least 10 min to remove possible oxo compounds formed on the nm-Ni/GC(*n*) surface. Cyclic voltammetric curves of nm-Ni/GC(*n*) with $n = 1$, 4, 12, 16, and 25 were then recorded between −0.9 and 0.5 V, while the solution was deaerated (Figure 4a). Two anodic peaks around −0.25 and 0.0 V were observed in the positive-going potential scan. These CV features can be attributed to the passivation of nm-Ni thin films.[39] The intensity of peak current (j_p), the peak potential (E_p), and the electric charge (Q_{Ni}) corresponding to the passivation of nanometer Ni films are listed in Table 3, which shows that both j_p and Q_{Ni} increase as *n* increases. Because the passivation of nanostructured Ni thin films occurs in positive-going potential scans, the cathodic current because of the reduction of surface oxide is relatively small; this can be seen clearly in the $j-E$ curve recorded in the negative-going potential scan (see Figure 4a).

The oxidation of CO adsorbed on newly prepared nm-Ni/GC(*n*) electrodes was carried out in the following way. (1) CO was bubbled into solution while undertaking potential cycling between −1.0 and −0.8 V with a new electrode for 10 min to

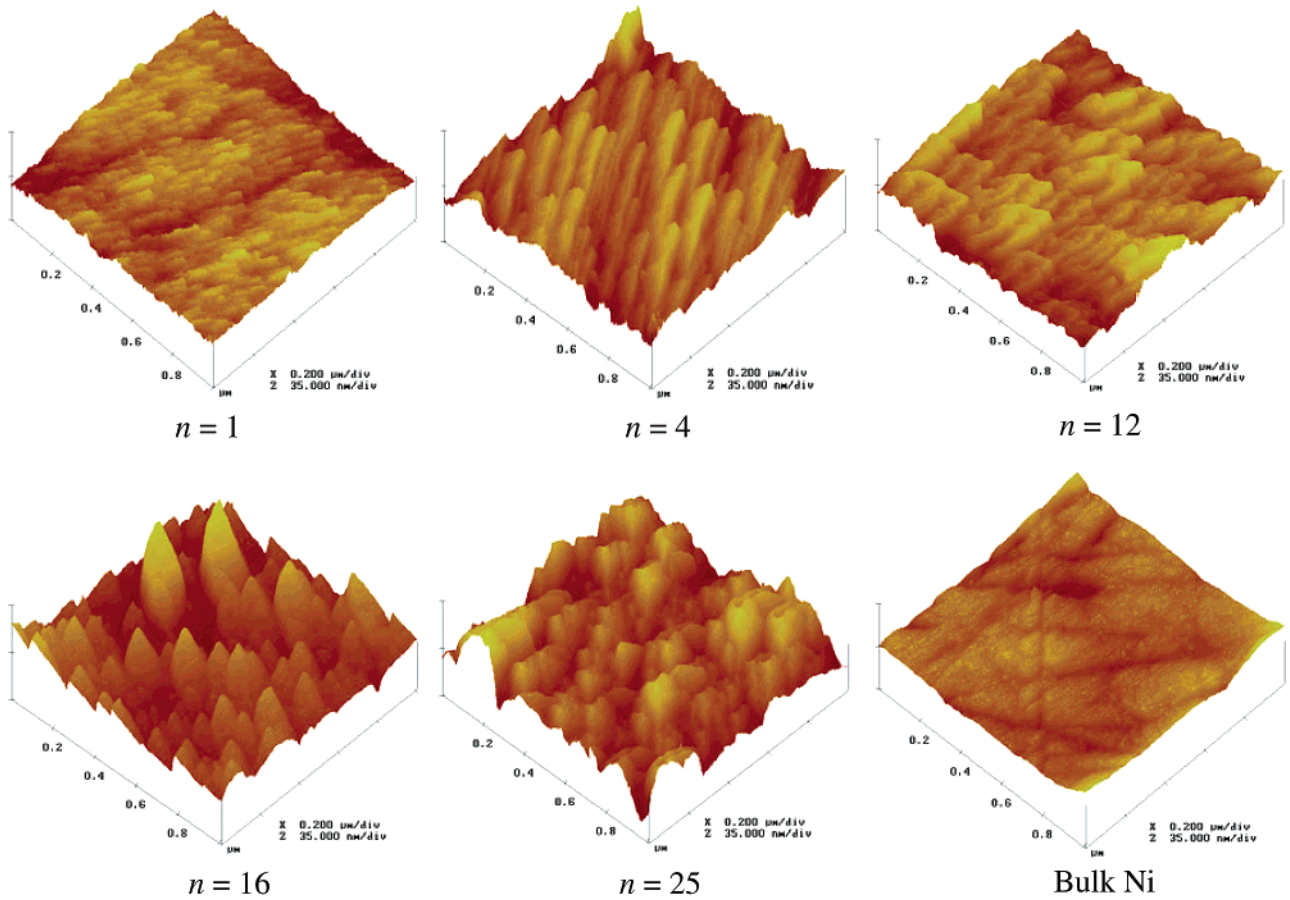

Figure 2. 3D structures of *in situ* STM images of nm-Ni/GC(n) with n = 1, 4, 12, 16, and 25 and bulk Ni electrodes.

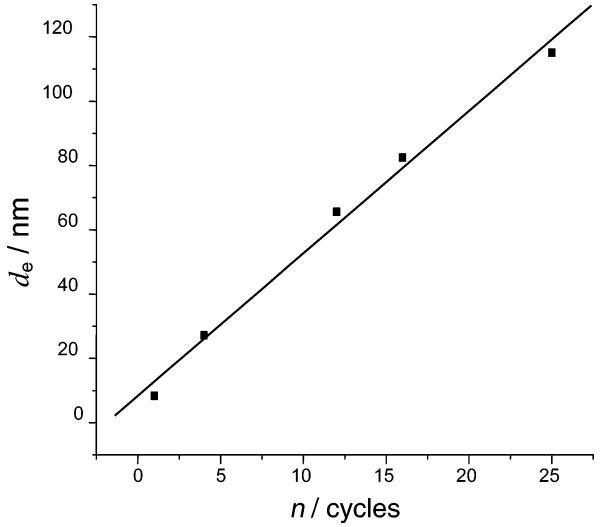

Figure 3. Relationship between the applied potential cycles (n) in electrodeposition and the estimated Ni film thickness (d_e).

TABLE 1: Variation of Q_d and d_e with n

n	1	4	12	16	25
Q_d (mC)	7.037	22.86	55.04	69.27	96.65
d_e (nm)	8.4	27.2	65.6	82.5	115.1

gain a saturation adsorption of CO on the electrode surface. (2) CO in the solution was removed completely by purging N_2. (3) The cyclic voltammograms of these electrodes between −0.9 and 0.5 V were recorded (Figure 4b). The anodic current peak around −0.25 V observed initially in Figure 4a has disappeared in Figure 4b demonstrating that the formation of a CO adlayer has retarded the oxidation and dissolution processes of Ni. An

TABLE 2: Variation of R_q with n

n	1	4	12	16	25	bulk Ni
R_q (nm)	2.4	3.9	4.2	7.4	10.9	2.3

anodic current peak can be observed in these voltammograms of electrodes studied in Figure 4b and can be attributed to the co-oxidation[42] of CO and Ni on nanostructured Ni thin films. Table 4 lists the E_p, j_p, electric charge of CO and Ni co-oxidation (Q_{CO-Ni}), and the full width at half-maximum (fwhm) of the current peak measured from voltammograms in Figure 4b. We can see that on nm-Ni/GC(*1*), j_p of amplitude 1.718 mA cm^{-2} appears at near 0.1 V with the corresponding fwhm of 161.7 mV. The current peak intensity is increased to 4.598 mA cm^{-2} at peak potential 0.17 V, and the fwhm is expanded to 227.4 mV when n is increased from 1 to 4. On further increases of n, E_p is shifted to 0.19 V and fwhm is slightly broadened, while j_p is decreased. It is interesting to see that Q_{CO-Ni} listed in Table 4 is much larger than Q_{Ni} of the corresponding nm-Ni/GC(n) electrodes reported in Table 3 and that for n = 4, 12, 16, and 25 Q_{CO-Ni} is almost about twice of the corresponding Q_{Ni}. In considering that the quantity of ($Q_{CO-Ni}-Q_{Ni}$) is much larger than the charge corresponding to the oxidation of a monolayer of CO adsorbed on metal electrodes,[33] the result may suggest that the oxidation of adsorbed CO on nm-Ni/GC(n) electrodes has promoted the passivation process of nanostructured Ni thin films. From the fact that similar anodic current peak intensities were measured for the co-oxidation of adsorbed CO and Ni on nm-Ni/GC(n) electrodes whether the solution is saturated or void of CO, it can be inferred (i) that CO must be securely adsorbed on nm-Ni/GC(n) electrodes, (ii) that only adsorbed CO is involved in the anodic oxidation, and finally (iii) that free CO

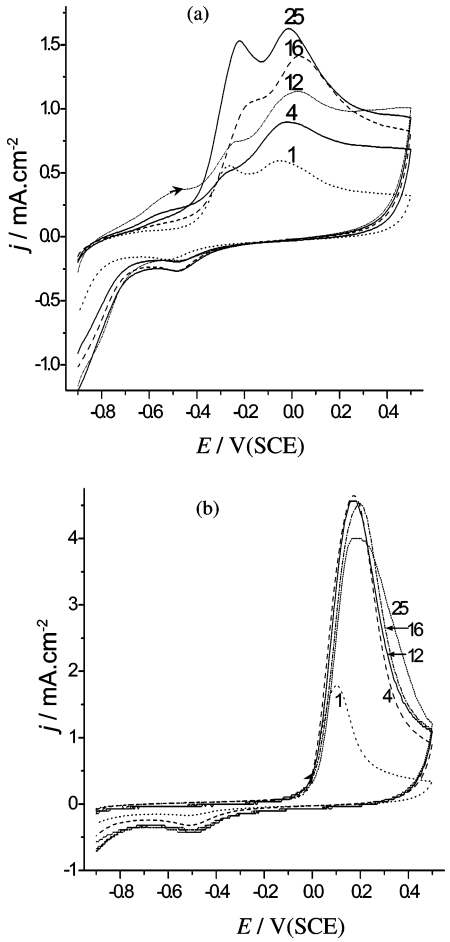

Figure 4. Cyclic voltammograms of nm-Ni/GC(*n*) electrodes with *n* = 1, 4, 12, 16, and 25, in 0.1 mol L^{-1} Na_2SO_4. (a) Native nm-Ni/GC(*n*) alone. (b) CO saturated on nm-Ni/GC(*n*) at a scan rate of 50 mV s^{-1}.

TABLE 3: Intensity of Peak Current (j_p), Peak Potentials (E_p), and Corresponding Electric Charges (Q_{Ni}) Measured in the Passivation of nm-Ni/GC(*n*) Electrodes

	E_p (V) (SCE)		j_p (mA cm^{-2})		
n	E_{p1}	E_{p2}	j_{p1}	j_{p2}	Q_{Ni} (mC cm^{-2})
1	−0.26	−0.05	0.471	0.489	8.00
4	−0.26	−0.02	0.365	0.711	13.03
12	−0.24	0.0	0.523	0.885	17.51
16	−0.18	0.03	0.807	1.080	17.85
25	−0.22	−0.01	0.987	1.177	21.78

TABLE 4: Intensity of Peak Current (j_p), Peak Potentials (E_p), Electric Charges (Q_{CO-Ni}) and fwhm of the Current Peak in the Co-oxidation of Adsorbed CO and Ni on nm-Ni/GC(*n*) Electrodes

n	E_p (V) (SCE)	fwhm (mV)	j_p (mA cm^{-2})	Q_{CO-Ni} (mC cm^{-2})
1	0.10	161.7	1.718	13.31
4	0.17	227.4	4.598	38.78
12	0.17	238.5	4.483	41.68
16	0.19	235.7	4.125	37.55
25	0.19	311.5	3.963	42.60

in the bulk solution could not be oxidized on an passivated Ni surface.

3. *In Situ* FTIR Spectroscopic Studies.

3.1 Results of MSFTIRS. In the MSFTIRS procedure,[40] single-beam spectra of sample potentials [$R(E_S)$] were collected for a series of E_S, under the conditions where CO is securely adsorbed on nm-Ni/GC(*n*) electrodes. The single-beam spectrum of reference potential [$R(E_R)$] was collected for the electrode

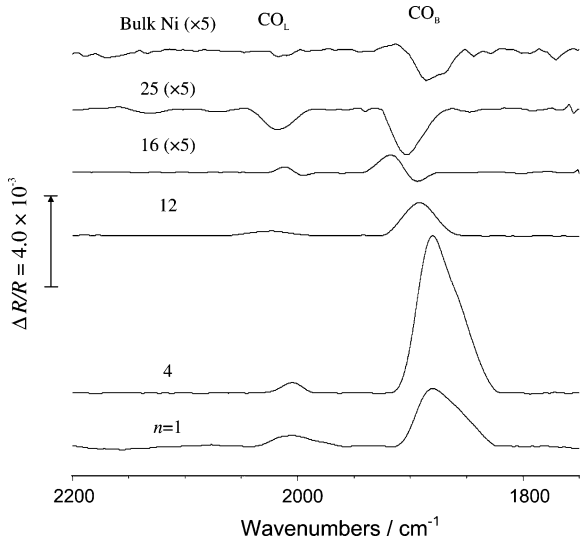

Figure 5. *In situ* MSFTIR spectra of CO adsorbed on nm-Ni/GC(*n*) with *n* = 1, 4, 12, 16, and 25 and bulk Ni electrodes. $E_S = -0.7$ V in 0.1 mol L^{-1} Na_2SO_4 solution.

surface stripped of CO. For the case of bulk Ni and nm-Ni/GC(*n*) with *n* = 1, 4, and 12, $R(E_R)$ was collected after an electrode is being polarized at 0.2 V for 15 s, so that CO_{ad} has been oxidized completely to CO_2. To avoid significant decreases of reflectivity of electrode surfaces caused by co-oxidation of Ni with CO, $R(E_R)$ of nm-Ni/GC(*n* = 16 and 25) was collected at −0.6 V before CO adsorption. Spectra recorded for all nm-Ni/GC(*n*) electrodes at $E_S = -0.7$ V are displayed in Figure 5, where for clarity, the ordinate scale for *n* = 16, 25, and bulk Ni is expanded by 5-folds. Because the IR absorption of CO_{ad} occurs only in $R(E_S)$, the resulted spectrum should yield CO_{ad} bands in a negative-going direction according to eq 1. This is clearly observed for the case of CO adsorbed on a bulk Ni electrode. Two negative-going bands near 2010 and 1880 cm^{-1} in the spectrum derived from bulk Ni can be observed and are attributed to IR absorption of linearly bonded CO (CO_L) and bridge-bonded CO (CO_B),[39] respectively. Remarkably, the direction of CO_{ad} bands is inverted completely and becomes positive-going in spectra of CO adsorbed on nm-Ni/GC(*n* = 1, 4, and 12) electrodes. As shown in Figure 1, these electrodes exhibit a layer nanostructure. In addition, the intensity of the positive-going CO_{ad} bands has been enhanced significantly in comparison to that observed in the spectrum of bulk Ni. The enhancement factor (Δ_{IR}) of CO adsorbed on nm-Ni/GC(*n*) is calculated by eq 3; the factor Δ_{IR} is defined by the ratio of the IR band intensity of the same amount of CO adsorbed on an nm-Ni/GC(*n*) to that adsorbed on a bulk Ni electrode[27]

$$\Delta_{IR} = \frac{(I_{CO}/I_{CO_2})_{nm-Ni/GC}}{(I_{CO}/I_{CO_2})_{Ni}} \quad (3)$$

where I_{CO} is the sum of the integrated intensity of the CO_L and CO_B bands and I_{CO_2} is that of the CO_2 band measured from spectra of bulk Ni and nm-Ni/GC(*n*) electrodes (Figure 6) recorded under the same experimental conditions. From IR spectra in Figures 5 and 6, Δ_{IR} has been determined to be 11.9, 15.5, and 2.7 for *n* = 1, 4, and 12, respectively. Further, the values of fwhm of the CO_B band in spectra of nm-Ni/GC(*n* = 1, 4, and 12) electrodes were measured to be 42, 44, and 35 cm^{-1}, which are broader than that measured on a bulk Ni electrode (30 cm^{-1}) by 12, 14, and 5 cm^{-1}, respectively. These IR features reveal that the nm-Ni/GC(*n* = 1, 4, and 12)

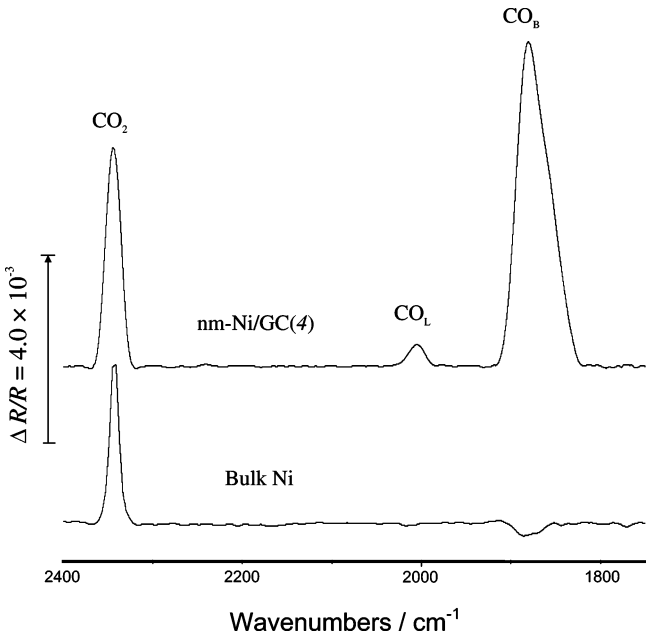

Figure 6. Comparison of *in situ* MSFTIR spectra of CO adsorbed on nm-Ni/GC(*4*) and that on bulk Ni electrodes. $E_S = -0.7$ V and $E_R = 0.2$ V in 0.1 mol L^{-1} Na_2SO_4 solution.

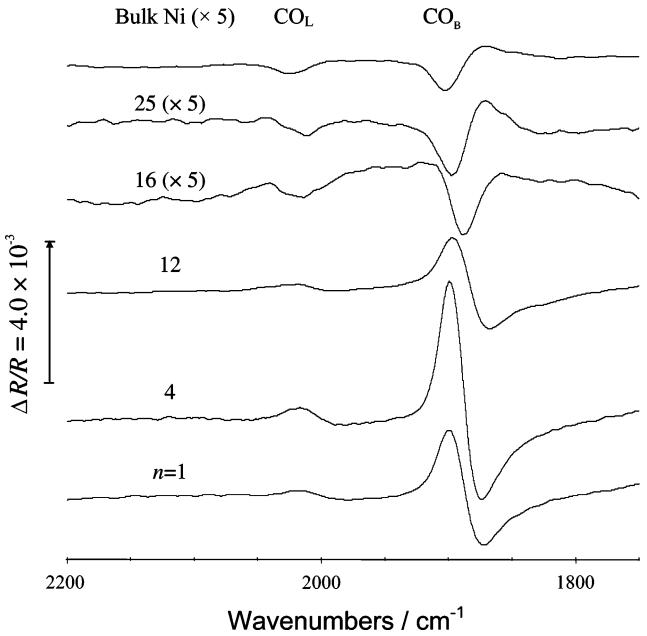

Figure 7. *In situ* SNIFTIR spectra of CO adsorbed on nm-Ni/GC(*n*) with $n = 1$, 4, 12, 16, and 25 and bulk Ni electrodes. $E_S = -0.7$ V and $E_R = -1.0$ V, 0.1 in mol L^{-1} Na_2SO_4 solution.

electrodes exhibit typical abnormal infrared effects (AIREs). To illustrate clearly the differences in IR features for CO adsorbed on bulk Ni and nm-Ni/GC($n = 1$, 4, and 12) electrodes, spectra recorded on nm-Ni/GC(*4*) and bulk Ni electrodes are compared in Figure 6; in contrast to the fact that the CO_2 band is positive-going in both spectra, the CO_{ad} bands in the two spectra appear in the opposite direction. Furthermore, the CO_{ad} bands in the spectrum of nm-Ni/GC(*4*) have been significantly enhanced and broadened. In correlating with STM results in Figure 1, we can conclude that Ni thin films possessing a layer nanostructure will display abnormal infrared effects. Previous studies have revealed also that nanoscale thin films of platinum group metals (such as Pt,[23] Ru,[24] and Rh[27]) prepared under cyclic voltammetric conditions also exhibit the AIREs as well as layer nanostructure.

It should be mentioned that the surface-enhanced IR absorption (SEIRA) may share some similar but not all characteristic IR features of the enhancement of IR bands of adsorbates. Osawa et al.[43] interpreted that the enhancement in SEIRA mainly arises from a strong electromagnetic field amplified through the excitation of collective electron resonance, as well some contribution of chemical interactions between the molecules and metal surface. However, such similarities are superficial; the AIREs and the SEIRA show different behavior in the following two aspects. (1) The direction of IR bands of absorbates is inverted in AIREs but remained the same in SEIRA. (2) The nanostructures for generating AIREs are made of continuous islands, while those electrodes for producing SEIRA consist of isolated nanoparticles.[44]

CO adsorbed on nm-Ni/GC(*n*) electrodes where $n = 16$ and 25 shows IR features very different from those observed on nm-Ni/GC(*n*) where $n = 1$, 4, and 12. A bipolar CO_L band with the negative peak near 1894 cm^{-1} and the positive peak around 1917 cm^{-1} appears in the former spectrum of nm-Ni/GC(*16*) as shown in Figure 5. This spectral line shape is somewhat similar to spectra referred to as the Fano coupling, which has been inferred to arise from the interaction of a discrete state with an energetically degenerate continuum.[45] While we continue to investigate the above phenomena and to identify their relation to Fano resonance, at present, we temporarily refer these features as "Fano-like IR features" (FLIRFs) because allied phenomena also have been recorded in other studies. These include those studies in transmission IR spectra of CO adsorbed on Fe film of several nanometers thickness hosted on Mg(001) under the conditions of ultrahigh vacuum,[46,47] ATR spectra of CO adsorbed on a 7-nm thin Pt film supported on silicon,[48] and those of CO adsorbed on electrochemically deposited Ru thin films supported on Pt metal.[34] In these studies, the structure of film and the size of nanoparticles in the film are both important parameters to yield the FLIRFs. In the present study, a Ni thin film that yields FLIRFs consists of island nanostructures with 82.5 nm thickness and islands of dimensions ranging between ~250−400 (length) × ~100−200 (width) × ~15−30 (height) nm.

When $n = 25$ in nm-Ni/GC(*n*), i.e., the Ni thin film possessing a lumpish arris nanostructure (Figure 1), the CO_{ad} bands are dramatically inverted to the negative-going direction; this pattern is the same to those observed in the spectrum of a bulk Ni electrode. The following SNIFTIRS studies should confirm these IR properties of nanostructured Ni thin films described above.

3.2 Results of SNIFTIRS. In contrast to the procedure of MSFTIRS, in the SNIFTIRS procedure, the spectra were collected at two potentials, i.e., −1.0 V as reference potential (E_R) and −0.7 V as sample potential (E_S); at both potentials, CO can be adsorbed securely on Ni surface. A total of 100 interferograms were collected respectively at E_R and E_S each time for the electrode potential being stepped from E_R to E_S. In total, 10 times of alteration between E_R and E_S were executed. The 1000 interferograms collected at E_R or E_S were co-added and Fourier transformed into single-beam spectrum $R(E_R)$ or $R(E_S)$. Resulted spectra of CO adsorbed on bulk Ni and nm-Ni/GC(*n*) surfaces were calculated using eq 1 and shown in Figure 7. For clear observation, the spectra recorded on nm-Ni/GC($n = 16$ and 25) and bulk Ni were expanded 5 times in the ordinate. Because of the Stark effect,[49] the infrared absorption of CO_{ad} at −0.7 V would be blue-shifted with respect to that at −1.0 V. As a consequence, the IR absorption of CO_{ad} will appear as bipolar bands with their positive peak in low

wavenumber side (IR absorption at −1.0 V) and negative peak on high wavenumber side (IR absorption at −0.7 V) in the resulted spectra calculated using eq 1. This is exactly the case of the spectrum recorded on a bulk Ni electrode, in which two bipolar bands are centered around 1880 and 2010 cm^{-1} and ascribed to IR absorption of CO_B and CO_L, respectively. However, IR absorption of CO adsorbed on nm-Ni/GC(*n*) electrodes displayed remarkable changes in IR features. Those nm-Ni/GC(*n*) ($n = 1$, 4, and 12) electrodes with layer nanostructure yield also bipolar bands, although their positive peak appears in high wavenumber side and the negative peak in low wavenumber side. It is evident that the direction of CO_{ad} bands is inverted and is the opposite to that in bulk Ni. Moreover, the intensity of CO_{ad} bands is enhanced, and the fwhm is expanded. These abnormal IR features confirmed that the nm-Ni/GC(*n*) with $n = 1$, 4, and 12 exhibit the AIREs as demonstrated previously in MSFTIRS studies. It is interesting to see that the intensity of the bipolar CO_{ad} bands is increased at first from $n = 1$ to 4 and then decreased when *n* increases continuously to 12.

Only negative-going monopolar CO_{ad} bands are observed in the spectrum recorded on the nm-Ni/GC(16) electrode that holds an island nanostructure. In considering the MSFTIRS results described above, this negative-going monopolar CO_{ad} bands appeared in SNIFTIRS spectrum correspond to Fano-like IR features. When *n* is increased further, i.e., on nm-Ni/GC(*25*) electrode, the spectral features become similar to those on bulk Ni electrode, i.e., bipolar CO_{ad} bands with their positive peak in low wavenumber side and negative peak on high wavenumber side. The SNIFTIRS study of CO adsorbed on nm-Ni/GC(*n*) electrodes also illustrated that the spectral IR features have undergone a transition from abnormal IR features to Fano-like IR features and finally to normal IR features along with *n* increasing progressively from 1 to 25.

Wu and co-workers[50] have simulated recently the fundamental of AIREs and FLIRFs by taking consideration of the interparticle interaction and electron−hole damping between nanoislands and CO molecules. The theoretical simulation shows that the islanded nanostructured Pt surfaces, which give rise to interparticle interaction, coupling with electron−hole mechanism, may contribute to the anomalous IR features of AIREs and FLIRFs. It may be worth pointing out that a complete understanding of the origin of the AIREs may involve exploration in different relevant disciplines and is still under investigation.

Conclusions

The current paper has extended the study of anomalous IR properties of nanostructured films originally discovered on platinum group metals to metal elements of the iron family. Electrochemical *in situ* STM studies illustrated that electrodeposition of Ni on glassy carbon [nm-Ni/GC(*n*)] under cyclic voltammetric conditions produced Ni thin films with different nanostructures along with the variation of film thickness. It has been observed that, following the increase of the number (*n*) of potential cycles applied in electrodeposition, the structure of Ni thin films is varied from layer nanostructure to island nanostructure and finally to lumpish arris nanostructure. The comparison of the charge of the co-oxidation of adsorbed CO (CO_{ad}) and Ni with the charge of Ni film passivation alone suggests that the oxidation of CO_{ad} may promote the passivation process of Ni thin films. Both *in situ* MSFTIRS and SNIFTIRS studies of CO adsorption on nm-Ni/GC(*n*) electrodes demonstrated that the IR properties depend strongly on the structure and thickness of Ni thin films, showing a transition from abnormal IR features ($n = 1$, 4, and 12) to Fano-like IR features ($n = 16$) and finally to normal IR features ($n = 25$). Together with the enhancement of IR absorption and the increase in width of CO_{ad} bands for CO adsorbed on nm-Ni/GC(*n*) electrodes, the present studies revealed that Ni thin films of the layer nanostructure exhibit abnormal IR effects, Ni films of island nanostructure possess Fano-like IR features, and thick Ni films of lumpish arris nanostructure display normal IR features that are similar to those observed on a roughened bulk Ni surface. The results obtained in the investigation are of importance in understanding the fundamental of anomalous IR properties of nanostructured film materials.

Acknowledgment. This work was supported by National Natural Science Foundation of China (Grants 90206039 and 20021002) and Chinese National Basic Research Program ("973" project, Grant 2002CB211804). We are grateful to Dr. Yuan L. Chow, Professor Emeritus, Simon Fraser University, Canada, for stimulating discussions.

References and Notes

(1) Pileni, M. P. In *Nanoscale Materials in Chemistry*; Klabunde, K. J., Ed.; John Wiley and Sons Inc.: New York, 2001; Chapter 2, p 61.
(2) Ferri, D.; Bürgi, T.; Baiker, A. *J. Phys. Chem. B* **2001**, *105*, 3187.
(3) Scott, W. J.; Datye, A. K.; Crooks, R. M. *J. Am. Chem. Soc.* **2003**, *125*, 3708.
(4) Khaleel, A.; Richards, R. M. In *Nanoscale Materials in Chemistry*, Klabunde, K. J., Ed.; John Wiley and Sons Inc.: New York, 2001; Chapter 4, pp 85−120.
(5) Awschalom, D. D.; Divincenzo, D. P. *Phys. Today* **1995**, *48*, 43.
(6) Ahmadi, T. S.; Wang, Z.-L.; Green, T. C.; Henglein A.; El-Sayed, M. A. *Science* **1996**, *272*, 1924.
(7) Weertman, J. R.; Averback R. S. In *Nanomaterials: Synthesis, Properties, and Application*; Edelstein, A. S., Cammarata, R. C., Eds.; Institute of Physics Publishing: London, U.K., 1996; Chapter 13, p 323.
(8) Gunther, L. *Phys. World* **1990**, *3*, 28.
(9) Ahmadi, T. S.; Wang, Z.-L.; Green, T. C.; Henglein, A.; El-Sayed, M. A. *Science* **1996**, *272*, 1924.
(10) Woltersdorf, J.; Nepijko, A. S.; Pippel, E. *Surf. Sci.* **1981**, *106*, 64.
(11) Wang, Z.-L. In *Characterization of Nanophase Materials*; Wang, Z. L. Eds.; Wiley-VCH Verlag GmbH: New York, 2000; Chapter 1.
(12) Ball, P.; Garwin, L. *Nature* **1992**, *355*, 761.
(13) Tabagi, H.; Ogawa, H. *Appl. Phys. Lett.* **1990**, *56*, 2379.
(14) Emory, R.; Haskins, W. E.; Nie, S. *J. Am. Chem. Soc.* **1998**, *120*, 8009.
(15) Osawa, M. In *Handbook of Vibrational Spectroscopy*; Chalmers, J. M., Griffiths, P. R., Eds.; Wiley: Chichester, U.K., 2002; Chapter 1.
(16) Lestowa, T. A.; Leyva-Lucero, M.; Mendez, E. R. *Opt. Commun.* **2000**, *183*, 529.
(17) Baldelli, S.; Epple, A. S.; Anderson, E. *J. Chem. Phys.* **2000**, *113*, 5432.
(18) Lu, G.-Q.; Sun, S.-G.; Chen, S.-P.; Li, N.-H.; Yang, Y.-Y.; Tian Z.-W. In *The Electrode Process VI*; Wieckowski, A., Itaya, K., Eds.; Electrochemcial Society Proceedings, 1996; Vol. 96, Chapter 36, p 436.
(19) Lu, G.-Q.; Sun, S.-G.; Chen, S.-P.; Cai, L.-R. *J. Electroanal. Chem.* **1997**, *421*, 19.
(20) Lu, G.-Q.; Sun, S.-G.; Chen, S.-P.; Cai, L.-R.; Tian, Z.-W. *Chem. J. Chin. Univ.* **1997**, *18*, 1491.
(21) Cai, L.-R.; Sun, S.-G.; Xia, S.-Q.; Chen, F.; Zheng, M.-S.; Chen, S.-P.; Lu, G.-Q. *Acta Phys.-Chim. Sin.* **1999**, *15*, 1023.
(22) Lu, G.-Q.; Cai, L.-R.; Sun, S.-G.; He, J.-X. *Chin. Sci. Bull.* **1999**, *44*, 1470.
(23) Lu, G.-Q.; Sun, S.-G.; Cai, L.-R.; Chen, S.-P.; Tian, Z.-W.; Shiu, K.-K. *Langmuir* **2000**, *16*, 778.
(24) Zheng, M.-S.; Sun, S.-G. *J. Electroanal. Chem.* **2001**, *500*, 223.
(25) Zheng, M.-S.; Sun, S.-G.; Chen, S.-P. *J. Appl. Electrochem.* **2001**, *31*, 749.
(26) Chen, Z.; Sun, S.-G.; Zhou, Z.-Y.; Ding, N. *Chin. Sci. Bull.* **2001**, *46*, 1439.
(27) Lin, W.-G.; Sun, S.-G.; Zhou, Z.-Y.; Chen, S.-P.; Wang, H.-C. *J. Phys. Chem. B* **2002**, *106*, 11778.
(28) Ortiz, R.; Cuesta, A.; Marquez, O. P.; Marguez, J.; Meadez, J. A.; Gutiérrez, C. *J. Electroanal. Chem.* **1999**, *465*, 234.
(29) Orazco, G.; Gutirrez, C. *J. Electroanal. Chem.* **1999**, *484*, 64.

(30) Bjerke, A. E.; Griffiths, P. R.; Theiss, W. *Anal. Chem.* **1999**, *71*, 1967.

(31) Bo, A.; Sanicharane, S.; Sompalli, B.; Fan, Q.-B.; Gurau, B.; Liu, R.-X.; Smotkin, E.-S. *J. Phys. Chem. B* **2000**, *104*, 7377.

(32) Bjerke, A. E.; Griffiths, P. R. *Appl. Spectrosc.* **2002**, *56*, 1275.

(33) Gong, H.; Sun, S.-G.; Chen, Y.-J.; Chen, S.-P. *J. Phys. Chem. B* **2004**, *108*, 11575.

(34) Gong, H.; Sun, S.-G.; Li J.-T.; Chen, Y.-J.; Chen, S.-P. *Electrochim. Acta* **2003**, *48*, 2933.

(35) Liao, B.; Lei, Y.-Q.; Lu, G.-L.; Chen, L.-X.; Pan, H.-G.; Wang, Q.-D. *J. Alloys Compd*. **2003**, *356*, 746.

(36) Lu, P.; Teranishi, T.; Asakura, K.; Miyake, M.; Toshima, N. *J. Phys. Chem. B* **1999**, *103*, 9673.

(37) Alvarez-Vega, M.; Garcia-Moreno, O.; Garcia-Alvardo, F.; Garcia-Jaca, J.; Gallardo-Amores, J. M.; Sanjuan, M. L.; Amador, U. *Chem. Mater.* **2001**, *13*, 1570.

(38) Mattei, G.; de Julian Fernandez, C.; Mazzoldi, P.; Sada, C.; De, G.; Battaglin, G.; Sangregorio, C.; Gatteschi, D. *Chem. Mater.* **2002**, *14*, 3440.

(39) Cuesta, A.; Gutierrez, C. *Langmuir* **1998**, *14*, 3397.

(40) Lin, W.-F.; Sun, S.-G. *Electrochim. Acta* **1996**, *41*, 803.

(41) Pons, S.; Davison, T.; Bewick, A. *J. Electroanal. Chem.* **1984**, *160*, 63.

(42) Ikemiya, N.; Suzuki, T.; Ito, M. *Surf. Sci.* **2000**, *466*, 119.

(43) Osawa, M.; Ikeda, M. *J. Phys. Chem.* **1991**, *95*, 9914.

(44) Sun, S. G. In *Catalysis and Electrocatalysis at Nanoparticle Surfaces*; Wieckowski, A., Savinova, E., Vayenas, C. G., Eds.; Marcel Dekker: New York, 2003; Chapter 21, pp 785−826.

(45) Fano, U. *Phys. Rev.* **1961**, *124*, 1866.

(46) Krauth, O.; Fahsold, G.; Magg, N.; Pucci, A. *J. Chem. Phys.* **2000**, *113*, 6330.

(47) Priebe, A.; Fahsold, G.; Pucci, A. *Surf. Sci.* **2001**, *90*, 482.

(48) Zhu, Y.; Uchida, H.; Watanabe, M. *Langmuir* **1999**, *15*, 8757.

(49) Lambert, D. K. *Electrochim. Acta* **1996**, *41*, 623.

(50) Wu, C.-X.; Lin, H.; Chen, Y.-J.; Li, W.-X.; Sun, S.-G. *J. Chem. Phys.* **2004**, *121*, 1553.